Materials Research Bulletin 150 (2022) 111768

Contents lists available at ScienceDirect

Materials Research Bulletin

journal homepage: www.elsevier.com/locate/matresbu

Research Papers

$ZrHfO_2$-PMMA hybrid dielectric layers for high-performance all solution-processed In_2O_3-based TFTs

M.G. Syamala Rao [a,b,*], K. Chandra Sekhar Reddy [a], J. Meza-Arroyo [a], Lakshmi N.S. Murthy [c], Trey B. Daunis [c], Maria Isabel Pintor-Monroy [c], Julia W.P. Hsu [c], R. Ramirez-Bon [a]

[a] Centro de Investigación y de Estudios Avanzados del IPN, Unidad Querétaro, Apdo, Postal 1-798, 76001 Querétaro, Querétaro, Mexico
[b] Facultad de Química, Posgrado en Ciencias de la Energía, Universidad Autónoma de Querétaro, 76010 Qro, Mexico
[c] Department of Materials Science and Engineering, The University of Texas at Dallas, 800 West Campbell Road, Richardson 75080, Texas, United States

ARTICLE INFO

Keywords:
Solution process
Thin films
Hybrid dielectric
Metal oxide semiconductor
Thin film transistor

ABSTRACT

Recently inorganic-organic hybrid materials have been quickly arisen as promising dielectric candidates for their applications in the fabrication of solution-processed metal oxide thin-film transistors (TFTs). Based on this, we demonstrate a novel mixed metal oxide hybrid dielectric layer of zirconium hafnium oxide-poly (methylmethacrylate) ($ZrHfO_2$-PMMA) thin films were effectively delivered by simple solution-process by using a low-cost spin coating process at a low temperature of 200 °C. To distinguish the chemical bonding states between inorganic and organic phases FTIR and XPS techniques were performed. The AFM analysis showed the hybrid thin films highly dense with low RMS roughness of around 1-nm. To investigate the dielectric properties of hybrid thin films, MIM capacitor devices were fabricated by using 90-nm thick hybrid dielectric layers exhibiting remarkably low leakage current density of 4.5×10^{-9} A/cm^2, capacitance density of 84.5 nF/cm^2 with high dielectric constant (k) of 8.4 at 1 kHz. Further, the hybrid dielectric layer was applied as a gate dielectric for fabrication of TFTs with solution processed In_2O_3 as the channel layer. All solution processed In_2O_3 TFTs showed an excellent electrical response with electron mobility of 11.2 cm^2/V. s, threshold voltage of 1.7 V, $I_{on/off}$ ratio of 10^6, and subthreshold swing of 0.58 V/dec. Therefore, our results illustrate the high potential of low-temperature solution processed $ZrHfO_2$-PMMA hybrid thin films for future low-cost TFT applications as gate dielectric candidate.

1. Introduction

The development of metal oxide thin film transistors (MOTFTs) by completely solution- process has been gaining a lot of attention for the enabling of low-cost future electronic devices. Recently, the solution processes have highly encouraged the research of new class of semiconductor and dielectric materials for their integration in TFTs [1–6]. Due to the economic, low-processing temperature, large area deposition and high-throughput characteristics, the solution processes offer to enhance the low-cost potential applications such as flexible displays, circuits, sensors, radio frequency identification tags (RFID) and stretchable electronics. According to the literature, significant research progress has been accomplished with several semiconductor and dielectric layers to achieve remarkable electrical performance of metal oxide TFTs. However, despite their excellent electrical performance, in the processing of most of the reported TFTs, at least one of the semiconductor or dielectric layer is deposited by high vacuum-based technique such as sputtering process [7–9]. On the other hand, chemical solution processes allow the device layers deposition by simple spin or dip coating methods at low-temperature, avoiding the use of expensive vacuum-based deposition techniques. This represents a great advantage for the cost reductions in electronics applications. Most of the attention on the solution-process approach has been focused on the metal oxide semiconductor layers for the fabrication of TFTs. Semiconductor active layers of zinc oxide (ZnO) [10], indium gallium zinc oxide (IGZO) [11], indium gallium tin oxide (IGTO) [12], tin oxide (SnO_2) [13] and indium oxide (In_2O_3) [14] deposited by solution processes have been shown excellent performance in TFTs. Among them, recently In_2O_3 has attracted enormous attention because of its advantages for the state-of-the-art TFT applications such as solution processing at low temperature (<250 °C), high electron mobility with good electrical stability [14–17]. These are highly promoting its use in TFT

* Corresponding author.
E-mail addresses: mullapudi.gouri@gmail.com (M.G. Syamala Rao), rrbon@cinvestav.mx (R. Ramirez-Bon).

https://doi.org/10.1016/j.materresbull.2022.111768
Received 20 August 2021; Received in revised form 4 December 2021; Accepted 25 January 2022
Available online 29 January 2022

devices.

With the rapid development of solution-processed metal oxide semiconductor layers, there is also a current necessity of dielectric layers synthesised by solution methods at low temperatures with enhanced dielectrical properties, to fulfill the requirements of fully solution-processed TFTs at low fabrication cost. Although most of the TFTs research has focused on the semiconductor active layers, the dielectric layers also play a critical role for accomplishing superior electrical performance in TFT devices. The electrical parameters of TFTs, including mobility (μ), threshold voltage (V_T), subthreshold swing (SS) and operating voltages not only depend on the semiconductor layer but also on the gate dielectric one. There are two main characteristics of the gate dielectric layer, which have strong influence on the TFTs electrical parameters. The first is the high capacitance to increase the accumulation of charge carriers at the semiconductor layer producing higher drain currents at lower operation voltages. This result in the enhanced mobility of the devices. The second one is the smooth, free-defects surface to enable the charge transport at the dielectric/semiconductor interface without charge trapping, which limits the drain current degrading the device mobility. Furthermore, this impact reduces the threshold voltages and subthreshold swing of the TFT devices [13]. Therefore, it is relevant the searching for new dielectric materials, which offers high capacitance and dielectric constant besides high-quality surface properties.

In recent times, several high-k dielectrics obtained by solution processes have been widely investigated as gate dielectric layers in metal oxide TFTs, including HfO_2, ZrO_2, Al_2O_3, Y_2O_3 and GaO_x [18–22]. Among these HfO_2 [23–26] and ZrO_2 [27–30] have received great importance by solution process and they are considered as feasible alternatives to SiO_2 gate dielectric because their high permittivity (k∼15–26), low leakage current and high thermal stability. Nevertheless, to accomplish the desirable dielectrical properties of these materials, it is required post deposition treatments at high annealing temperatures above 400 °C, which is an important limitation for the growth of high-quality dielectrics by low-cost solution process. The combination of two high-k binary metal oxides to obtain ternary alloys such as HfAlOx, ZrAlOx, YAlOx, HfGdOx and ZrGdOx [31–35], is truly picking up the interest to further improvements in the dielectric properties of the high-k metal oxide dielectrics. However, despite of the remarkable progress achieved by developing these ternary inorganic dielectrics with emerging methods such as water solvents or UV photo annealing methods [36], still they require temperatures above 200 °C to ensure the development of dense thin films with superior dielectric properties. Moreover, their brittleness is often not compatible with temperature sensitive plastic substrates employed for flexible electronic devices.

To conquer those inherent limitations of solution processed high-k inorganic dielectrics, recently several dielectric materials have been investigated as gate dielectrics layers. In this, crosslinking polymers are receiving great attention owing to their low temperature solution processing. However, most of these polymer-based insulators are particularly applied as gate dielectrics for organic TFTs (OTFTs) [37]. Even though their excellent solution processability at low temperatures, polymer dielectrics suffer from high thickness and high leakage currents, which deteriorates their electrical performance, particularly increasing the operating voltages, and lowering the carrier mobilities in the devices. Recently, hybrid approach such as inorganic-organic hybrid dielectrics are emerging as alternative gate dielectric layers for metal oxide TFTs applications. Hybrid materials are the blend of inorganic and organic phases with a crosslinking molecule, which in a synergistic way combine the properties of both components [38]. As a result, hybrid materials take advantage of the high dielectric constant (k), high capacitance and low leakage current of the inorganic phase as well as the solution processability at low temperatures, typically in the range of 100–200 °C, and mechanical properties of the organic dielectric polymers [38,39]. For these reasons, we have applied this hybrid approach to synthesize inorganic-organic hybrid dielectric layers utilizing silane-based coupling agents to combine both phases through strong covalent bonds and obtained by one-step spin or dip coating process at low temperature. In addition, these crosslinked hybrid dielectrics offer a smooth, pinhole-free, and uniform surface with excellent dielectric features, such as low leakage current and high permittivity correlated to the high-k oxide dielectrics as the inorganic phase. So far, very less research has been reported on hybrid dielectric materials for metal oxide TFTs, particularly for solution based In_2O_3 TFTs.

Recently, our group developed several hybrid dielectrics layers such as HfO_2-PMMA, $ZrHfO_2$-PMMA, Al_2O_3-GPTMS-PMMA and HfO_2-GPTMS by low temperature solution processing and successfully applied them to sputtered ZnO and IGZO-based TFTs in our previous reports [40–43] with excellent electrical performance. These hybrid dielectric layers were based on high-k metal oxides as the inorganic component and PMMA as the organic one. In the present research, we report the further development of the inorganic-organic hybrid gate dielectric constituted by the combination of hafnium and zirconium inorganic oxide compounds blended with poly(methylmethacrylate) (PMMA) as the organic phase. The mixed metal-oxide $ZrHfO_2$-PMMA hybrid dielectric layers were deposited by sol-gel process by using 3-glycidoxy propyl trimethoxy silane (GPTMS) as cross-linker. Unlike our previously reported $ZrHfO_2$-PMMA hybrid dielectric layers for IGZO and ZnO-TFTs [41], after thermal annealing at 200 °C to cross-link the inorganic and organic phases, the mixed-oxide hybrid films were subsequently treated with UV-ozone for 10 min to modify the hybrid dielectric surface for better interface to deposit the semiconductor channel layer. The resulting hybrid dielectric layers were highly transparent with very smooth surface and enhanced dielectric properties. Then, we utilized these hybrid dielectric layers to establish a fully solution-based processing of TFTs with In_2O_3 as the semiconductor channel layer. The assembling of the bottom-gate structured TFTs on ITO-coated glass substrate started with the dielectric gate hybrid layer deposition, followed by the deposition of the In_2O_3 channel layer by spin coating method. The analysis of the electrical response of the devices revealed that the fully solution-processed In_2O_3-based TFTs featured outstanding electrical performance, including high field effect saturation mobility of 11.2 $cm^2V^{-1}s^{-1}$, large on/off current ratio 10^6, threshold voltage of 1.7 V, and subthreshold swing of 0.58 V/dec. These results are quite competitive as compared with other hybrid gate dielectrics for In_2O_3–based TFTs applications [44,45].

2. Experimental details

2.1. Synthesis of hybrid dielectric and semiconductor precursor solutions

To prepare the sol-gel hybrid solution for the deposition of the hybrid dielectric films, we closely followed our previously reported synthesis [41]. The inorganic precursor solution was prepared by using hafnium chloride ($HfCl_4$, 98%) and zirconium chloride ($ZrCl_4$, 99.99%). These precursors were dissolved in ethylalcohol (99.99%). Afterwards, nitric acid (HNO_3 65.1%) and deionized (DI) water were added one by one into this precursor solution to keep the final concentration of the solution with 1:100:10:10 molar ratio, then vigourously stirred for 4 hrs at 60 °C to promote the hydrolysis and condensation processes of the inorganic network [40,41]. To prepare the cross-linking solution, 3-glycidoxypropyl trimethoxysilane (GPTMS 98%) was hydrolized in 2-propanol (99%) and a small amount of nitric acid (HNO_3 65.1%) was added into this mixture to catalyze the reactions in the solution [46]. The final mixture was stirred for 1 hr at room temperature. For the organic PMMA precursor solution, benzoyl peroxide (BPO 98%) was used to start the polymerization of MMA and the obtained solution was stirred for 3 hrs at 70 °C [42]. The optimized final concentration of the hybrid precursor solution was fixed at 2:1:1:1molar ratio with respect to Zr:Hf:GPTMS:PMMA. The resulting transparent $ZrHfO_2$-PMMA hybrid solution was stirred for more than 4 hrs at room temperature to complete the hybrid

sloution formation. For the synthesis of the In_2O_3 semiconductor films, the precursor indium nitrate hydrate ($In(NO_3)$ x.H_2O) was dissolved in 2-methoxyethanol solvent and acetylacetone was used as stabilizer. The final concentration of the solution was fixed at 0.2 M and stirred for over night at room temperature. All the reactives were received from Sigma-Aldrich and they were used without any further purification.

2.2. Deposition of hybrid dielectric thin films

Before the deposition of the hybrid dielectric thin films, the acquired transparent hybrid solution was filtered through a 0.2 μm syringe PTFE filter. Then, the hybrid solution was dropped on various types of substrates to deposit the hybrid films by a simple spin coating process at 5000 rpm for 30 s. After deposition, the as-spun hybrid dielectric thin films were placed immediately on a hot plate at 100 °C to evaporate the organic residual solvents and then thermally annealed at 200 °C for 12 hrs to cross-link the hybrid thin films in air environment [40,41]. Then the $ZrHfO_2$-PMMA hybrid films were further treated by UV-ozone for 10 min to eleminate remaining organic residuals on the hybrid surface to further improve the film quality and surface wettability. The scheme of the hybrid dielectric film deposition process is shown in Fig. 1.

2.3. Hybrid thin film characterization and MIM device fabrication

The hybrid thin films were characterized by thermogravimetric analysis, TGA (Perkin Elmer, Model Pyris 1), Fourier-transform infrared spectroscopy, FTIR (Perkin Elmer, Model GX), X-ray photoelectron spectroscopy, XPS (Intercovamex, Model Alpha 110), atomic force microscopy, AFM (Nanoscope) and field emission scanning electron microscope, FE-SEM (JEOL-JSM-1670F) to assess their thermal, structural, chemical, and morphological properties. The electrical characterization of the 90-nm thickness hybrid thin films were carried out on MIM capacitor devices fabricated on ITO-coated glass substrates with evaporated gold contacts as top electrodes by shadow mask process. The capacitance versus voltage measurements (*C-V*) were carried out on a HP 4284 A precision LCR meter at frequency ranging from 1 kHz to 1 MHz, and the leakage current density (*I-V*) was measured at an applied bias voltage from −5 V to 5 V by using a 4200 Keithley semiconductor parameter analyser in ambient conditions.

2.4. Deposition of In_2O_3 thin films and TFT fabrication

For the fabrication of bottom-gated In_2O_3-based TFTs, the hybrid dielectric gate layer was first deposited on ITO-coated glass substrates as mentioned above. Subsequently, the solution processed In_2O_3 semiconductor channel layer was deposited on top of the hybrid dielectric gate by spin coating process at 3000 rpm for 30 s. The thin film was dried at 80 °C for 1 min in a hot plate and then exposed to UV-ozone treatment for 10 min. This process was repeated one more time to reach the desired film thickness of 13–15 nm (measured by ellipsometry). Then, the In_2O_3 thin film was first annealed at 150 °C for 5 min followed by other at 220 °C for 20 min on a hot plate to densify it [32], as shown in Fig. 1. Finally, 200 nm-thickness aluminum (Al) source and drain electrodes were patterned on top of the semiconductor layer by e-beam evaporation (Temescal BJD-1800) through a shadow mask. For the electrical characterization of the In_2O_3-based TFTs, current versus voltage curves were measured in a 4200 Keithley semiconductor parameters analyser in a dark ambient atmosphere. The evaluation of the field effect mobility in the saturation region and the other electrical parameters were extracted from the transfer curve characteristics of the TFTs by using the following equation [41]:

$$I_{DS} = \frac{W\ \mu\text{sat}\ CG}{2L}\ (V_{GS} - V_{th})^{\ 2} \quad (1)$$

where I_{DS} is the drain to source current, W and L are the width and length of the channel, C_G is the dielectric gate capacitance, μ_{sat} is the device mobility, V_{GS} is the gate to source voltage and V_{th} is the threshold voltage.

3. Results and discussion

Fig. 1 demonstrates the schematic of the fully solution thin-film transistors (TFTs) fabrication process, assembled with the mixed metal-oxide hybrid dielectric ($ZrHfO_2$-PMMA) as gate insulator and indium oxide (In_2O_3) as semiconductor channel layer. Both dielectric and semiconductor layers were deposited by a simple spin coating method in a bottom gate/top contact TFT structure. The highest temperature in the TFT fabrication process was 220 °C. In order to achieve better electrical performance in the TFTs, the dielectric gate properties play an essential role, where the high dielectric constant and low leakage current are among the most important. In this report, we focused primarily on the synthesis of the hybrid dielectric layers, their deposition process by low temperature sol-gel method and the analysis of their properties to determine the potential applicability as gate dielectric in TFTs.

In order to investigate the thermal behavior of the hybrid material, thermogravimetric analysis (TGA) was carried out to identify the thermal stability and structural transformation. Fig. 2 shows the TGA plot of the hybrid material powder obtained from its hybrid precursor solution dried at 200 °C for 12 h to evaporate the organic residuals. The TGA curve displays three main steps of weight loss at various temperature zones labeled as I, II and III, respectively. The first weight loss occurs at the temperature interval between 50 °C and 190 °C, which was mainly attributed to the evaporation of water and the decomposition of other remaining organic solvents, which were used in the sol-gel method to promote the hydrolysis and condensation processes. After this temperature there is still 4% solvents remaining in the hybrid material due to low annealing temperature process, which may act as traps in the hybrid material. Subsequently, the metal hydroxides are transformed into metal oxides such as HfO_2 and ZrO_2 by dehydroxilation process. The subsequent second weight loss starts at around 220 °C and it was gradually continuous up to 600 °C. This sudden weight loss is related to the degradation of the PMMA polymer and remaining hydroxyl residuals

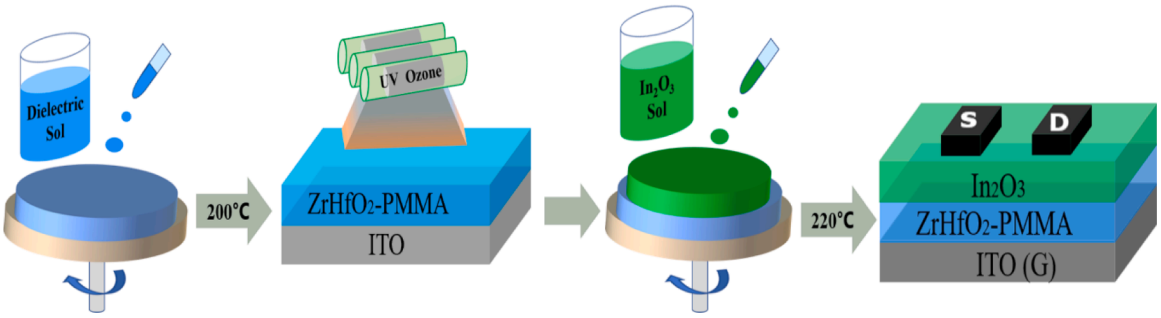

Fig. 1. Schematic of precursor solutions deposition of hybrid dielectric and semiconductor layers for the fabrication In_2O_3 TFT.

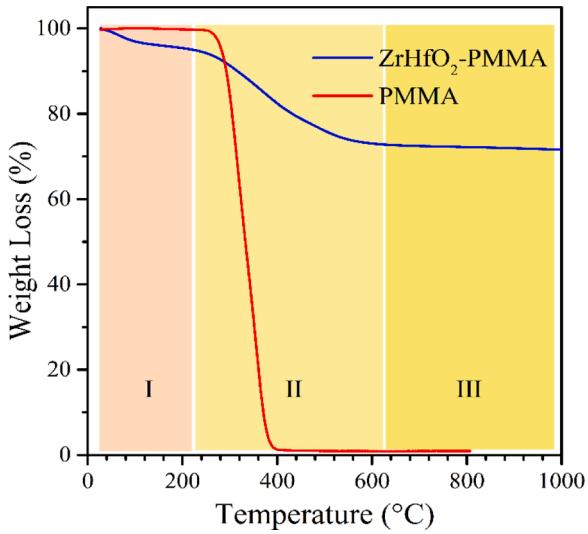

Fig. 2. Thermogravimetric analysis (TGA) curve of the hybrid $ZrHfO_2$-PMMA powder. For reference it is included the corresponding TGA curve for pristine PMMA.

still present in the hybrid material. The pristine PMMA completely decomposes at the temperature around 400 °C [41,47] as shown by the dotted line curve. In contrast, in the hybrid material there is an amount of organic polymer phase still existing, which requires higher temperature to decompose up to 600 °C, as evidenced by the TGA curve. This corresponds to the loss of organic phase linked with the inorganic one, which requires higher temperature to release from the hybrid material as compared with the polymer chains without interactions. The observed increased thermal resistance of the organic phase in the hybrid material has been ascribed to the strong link between their organic and inorganic phases. This way, the total content of organic phase in the hybrid material is 23%. In the third step, at temperatures above 600 °C, there is no noticeable weight loss, which indicates that the organic decomposition process was completed. Therefore, the remaining weight of the hybrid material at the highest temperature, around 73%, corresponds to the thermally stable inorganic metal oxides. This is signifying that the resultant hybrid material is inorganic-rich, which is desirable to obtain superior dielectric properties. From the aforementioned discussion of TGA analysis, it is clearly observed that the precursors transformation completes nearly to 200 °C to successfully form the hybrid matrix.

Fig. 3a) and 3 b) shows the FTIR spectra of the $ZrHfO_2$-PMMA hybrid thin film in different spectral ranges. In Fig. 3a), the characteristic absorption band at 3462 cm^{-1} can be assigned to stretching vibration modes of surface hydroxyl groups produced in the inorganic part in the form of M-OH (*M*=Hf, Zr). The other two weak absorption bands observed at 2938 and 2885 cm^{-1} are assigned to symmetric and asymmetric -CH_2 vibrations, respectively, which are present in the cross-linker GPTMS molecules [43]. The low intensity broad bands centered at 1640 and 1436 cm^{-1} correspond respectively to C = O stretching and C—O vibrations of carbonate groups from the PMMA organic phase [40]. The strong and sharp band centered at 1129 cm^{-1} can be assigned to Si-O-C or M-O-Si stretching modes, evidencing that the GPTMS cross-linker molecules react with the PMMA polymer or the metal inorganics chemical reaction with the GPTMS cross-linker [43, 48]. This is indicating the strong interaction through chemical bonds between both inorganic and organic counter parts for the formation of the stable hybrid network. On the other hand, in Fig. 3b) the sharp high intensity vibration band at 372 cm^{-1}, as well as the low intensity peak at 421 cm^{-1} can be assigned to the ionic character of the Zr-O bond and the other bands at 389 and 408 cm^{-1} are related to vibration modes of Hf-O bonds [41] in the inorganic phase.

To investigate more deeply the core level chemical bonding states of the elements in the solution-processed $ZrHfO_2$-PMMA hybrid films, XPS (Fig. 4) measurements were performed to confirm the inorganic-organic hybrid network formation. As observed in Fig. 4a), the survey scan spectrum of the hybrid film displays the signals corresponding to all the expected elements (Hf 4f, Zr 3d, O 1 s, C 1 s, Si 2p) incorporated in the hybrid material. The individual core level spectra of these elements are shown in Fig. 4b)-f). In Fig. 4b), the Zr 3d spin doublet spectrum can be deconvoluted into two major peaks at the binding energies of 184 and 186.3 eV. The first peak is related to Zr 3d5/2 and the other one to Zr 3d3/2. Both peaks are shifted towards higher binding energies, which strongly indicates the formation of Zr-O, and Zr-O-Si bonds via condensation reactions of Zr-OH moieties reacted with silane GPTMS cross-linking precursor [7, 41]. Fig. 4c) shows the Hf 4f spectrum and its deconvolution into several peaks located at the binding energies of 18.7, 19.5, 20.3 and 21.1 eV, which correspond to Hf-O bonds [49] and the other peak at lower binding energy of 17.8 eV is related to Hf-O-Si bonds [50]. Here, the chemical state of Hf-O-Si bond suggests that the inorganic phase of Hf-O reacted with the GPTMS molecules to form a strong cross-linked hybrid network in the dielectric thin film. Fig. 4d) shows the O 1 s spectrum deconvoluted into four peaks. The strong dominant peak at 529.1 eV is associated to C—O bonds evidencing the presence of the organic phase [51]. The high intensity peaks at 529.9 eV and 530.6 eV binding energies are attributed to the formation of M-O (*M*= Hf and Zr) bonds [38]. The low intensity peak at 531.5 eV is related to C = O bonds constituting the polymer within the hybrid network or unreacted Si-OH groups [51, 52] still existing in the hybrid film due to the incomplete condensation reactions. Normally, these hydroxyl groups act

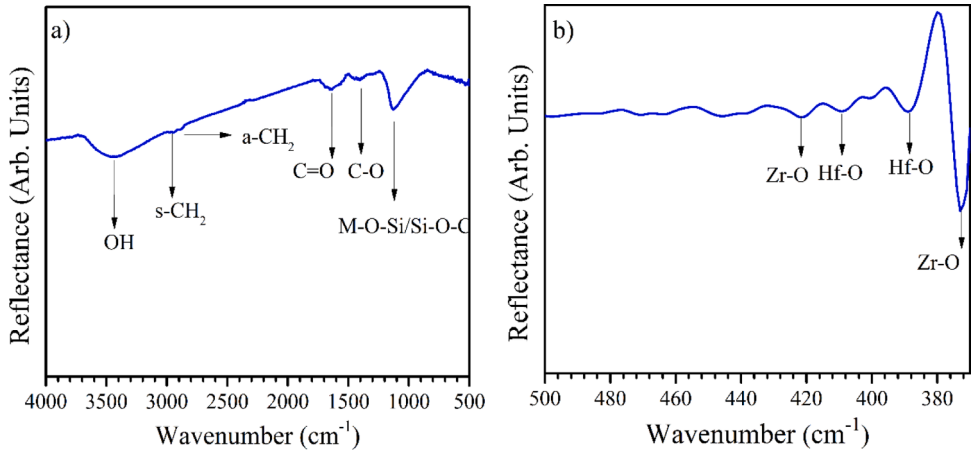

Fig. 3. FTIR spectra of $ZrHfO_2$-PMMA hybrid thin film in the wavenumber range of a) 4000–500 cm^{-1} and b) 500–370 cm^{-1}.

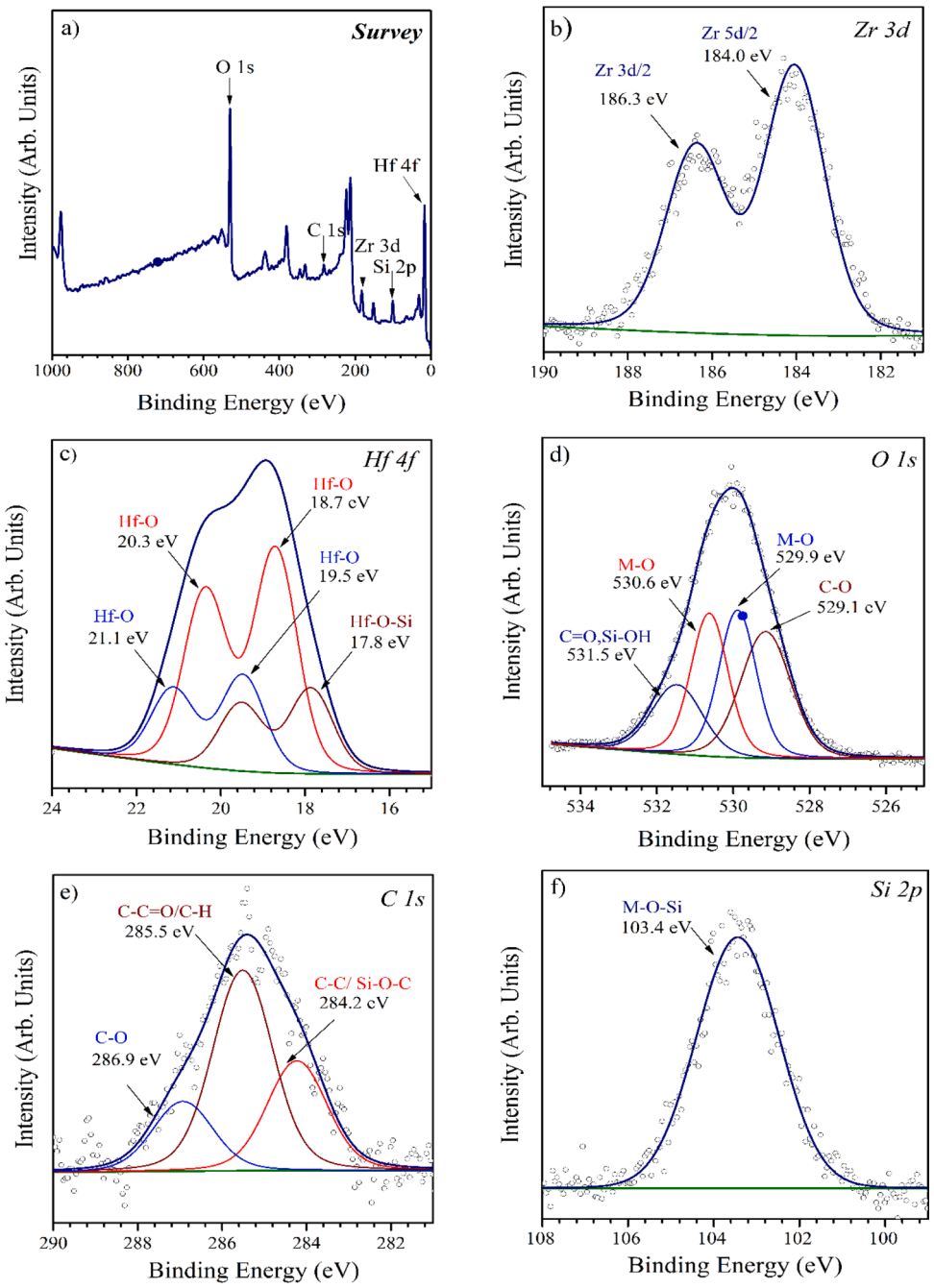

Fig. 4. XPS analysis of the hybrid dielectric layer: a) wide scan, b) Zr 3d, c) Hf 4f, d) O 1 s, e) C 1 s and f) Si 2p spectra.

as traps influencing the electrical properties of the hybrid dielectric films. In Fig. 4e) the C 1 s spectrum is deconvoluted into three main peaks, the peak at 284.2 eV corresponds to C—C or Si-O-C bonds [46]. The high intensity peak at 285.5 eV is due to C—C = O bonds and the other at 286.9 eV is related to the C—O ones [51]. Therefore, all the C 1 s peaks reveal the presence of the organic polymer and the interaction with the cross-linking agent. Fig. 4f) represents the Si 2p spectrum where the peak at binding energy of 103.4 eV can be allotted to the M-O-Si bonds [50]. Finally, the overall XPS analysis indicates the successful formation of the organic-inorganic hybrid network, in agreement with the FTIR results.

The surface characteristics of the hybrid thin film, which have strong influence on their dielectric properties, were observed by AFM. Fig. 5 shows the a) $ZrHfO_2$-PMMA hybrid dielectric and b) pure PMMA polymer thin film surface morphologies, measured by AFM in tapping mode over a 3 × 3 μm^2 scan area. The AFM images display the optimized surface morphology of the UV-cured hybrid dielectric thin film with very homogeneous, smooth, and pinhole-free surface. The root-means-square (RMS) surface roughness measured in the scanned area of the hybrid film was very low, around 1nm. Besides, the PMMA polymer surface roughness increased little bit to the RMS roughness value of 1.44 nm. Such a low surface roughness of the hybrid films is promising to achieve enhanced dielectric properties. This is also highly beneficial for the growth of semiconductor layers on this dielectric surface to reduce the charge scattering at the dielectric/semiconductor channel interface, improving the electron charge transport in the channel layer and thereby the electrical performance parameters in TFTs, such as high mobility and low SS [53]. Additionally, to know hybrid dielectric surface chemical nature, contact angle measurements were done to estimate its surface energy. For this, the contact angles were measured by

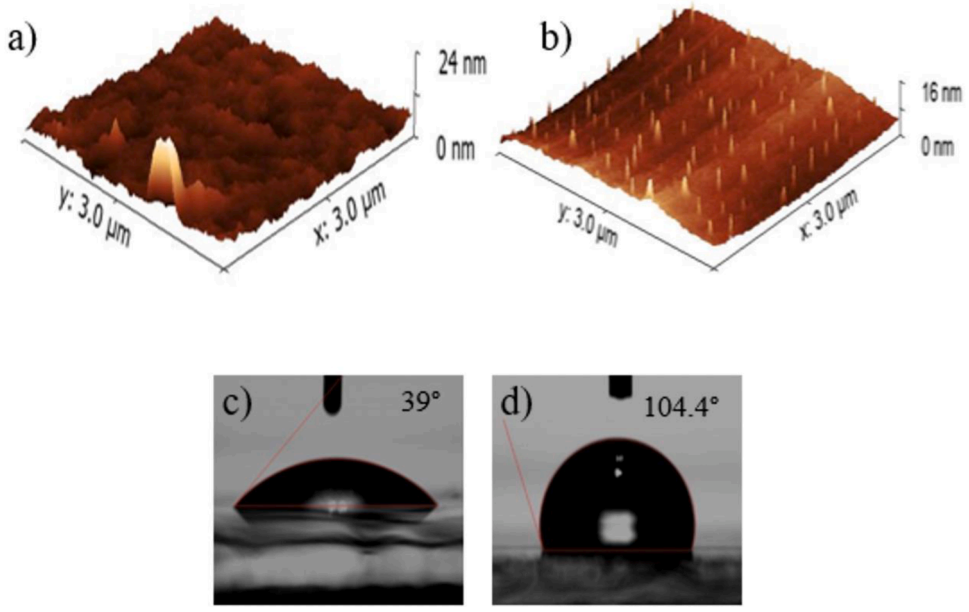

Fig. 5. AMF tapping mode height image of a) $ZrHfO_2$-PMMA hybrid dielectric b) polymer PMMA dielectric and water contact angle measurements of c) before UV-Ozone and d) after UV-Ozone treatment on the hybrid dielectric surface.

using three special liquid droplets as test liquids such as water, ethylene glycol and diiodomethane on the hybrid film surface before and after UV-ozone treatment. For water, the measured contact angles were found to be 39° and 104.4° as shown in Fig. 5(c) and (d), respectively. The strong increase of the water contact angle after the UV-Ozone treatment was observed in these optical images revealing the transformation from hydrophilic to hydrophobic behavior of the hybrid film surface. By applying the UV-ozone treatment on the hybrid surface, it makes the extensive photon energy generated by the UV irradiation, then the active oxygen species dissociate the unreacted organic compounds in the film and strongly oxidize the suboxides to form metal oxides (M-O) bonds, thereby removing such defects and oxygen vacancies present in the film. This implies that the UV-ozone treatment makes the $ZrHfO_2$-PMMA hybrid dielectric film more nonpolar dielectric surface by reducing the amount of complex hydroxyl groups (-OH) [54,55]. The surface free energy of the hybrid dielectric was determined from the measured contact angles by employing the following geometric mean model equation [52].

$$\gamma_l(1+\cos\theta_l) = 2\left(\sqrt{\gamma_l^d \gamma_s^d} + \sqrt{\gamma_l^p \gamma_s^p}\right) \quad (2)$$

where θ_l is the droplet angle formed between the liquid and gate dielectric layer. γ refers to surface energy, the superscripts *d* and *p* represent the dispersive and polar components of the surface energy. Meanwhile, the subscripts *l* and *s* indicate the energy related to the liquid and solid (film), respectively. The estimated surface free energies for the obtained hybrid film before and after the UV-ozone treatment were 59.1 mJ/m^2 and 26.7 mJ/m^2, respectively. These results are presented in the Table 1. Generally, hydrophilic surfaces with high surface energy are not favorable for the growth of semiconductor films by solution process due to its highly polar groups, which act as charge trapping sites limiting the charge carrier transport and then degrading the device electrical performance. Thus, a low dielectric surface energy of hybrid dielectric can enhance the TFT performance with reliable electrical properties [54].

Table 1
Contact angle and surface energy measurements of $ZrHfO_2$-PMMA hybrid dielectric before and after UV-ozone treatment.

Dielectric $ZrHfO_2$-PMMA	Contact Angle			γ_s^p(mJ/m^2)	γ_s^d(mJ/m^2)	($\gamma_s^p + \gamma_s^d$)(mJ/m^2)
	Water	DM	EG			
Without UV-Ozone	39	48.8	32.3	35.5	23.6	59.2
With UV-Ozone	104.4	73.8	80.4	0.9	25.8	26.7

To investigate the electrical properties of the hybrid dielectric films, metal-insulator-metal (MIM) capacitor devices were assembled on ITO and gold circular contacts as bottom and top electrodes, respectively, as shown in the schematic structure of Fig. 6a). These devices were used to measure the hybrid films electrical characteristics such as dielectric leakage current and capacitance. Fig. 6b) represents the FESEM cross-section image of the $ZrHfO_2$ -PMMA hybrid dielectric layer where the measured physical thickness is about 90 nm. Fig. 6c) shows the leakage current density versus voltage plot (*I-V*) of the hybrid dielectric film. As shown in this graph, the leakage current density measured in the hybrid dielectric film is as low as 4.3×10^{-9} A/cm^2 at an applied voltage of both negative and positive −5 V to 5 V. The exhibited low leakage current density of the hybrid dielectric is considerably lower than that measured in our previously reported $ZrHfO_2$-PMMA hybrid dielectric layer [40], and in other reported high temperature solution processed inorganic dielectrics [19,22]. The found low leakage current density is attributed to the surface UV-ozone treatment on the hybrid dielectric surface, which considerably reduced the surface hydroxyl groups and oxygen vacancies in the hybrid thin film. The UV-ozone radiation reacts with oxygen in the ambient air to convert into reactive oxygen species. These reactive oxygen species diffuse into amorphous sol-gel film to fill the oxygen vacancies in the hybrid film [55,56]. Additionally, the active oxygen species dissociate the unreacted organic compounds in the hybrid film and strongly oxidize the suboxides to form metal oxides (M-O) bonds, thereby reducing such defects hydroxyl groups (OH) [56]. The low leakage current density is highly desirable for the fabrication of stable TFTs for low power consumption electronic devices. In addition, the capacitance density of the hybrid dielectric was measured on the same MIM device in the frequency range from 1 kHz to 1 MHz and the results are presented in Fig. 6d). As noted, the capacitance density decreased at higher frequencies probably due to the slow orientation of polarization response, which requires longer time response at higher frequencies. Finally, the dielectric constant of hybrid dielectric is calculated by using the following equation [43]:

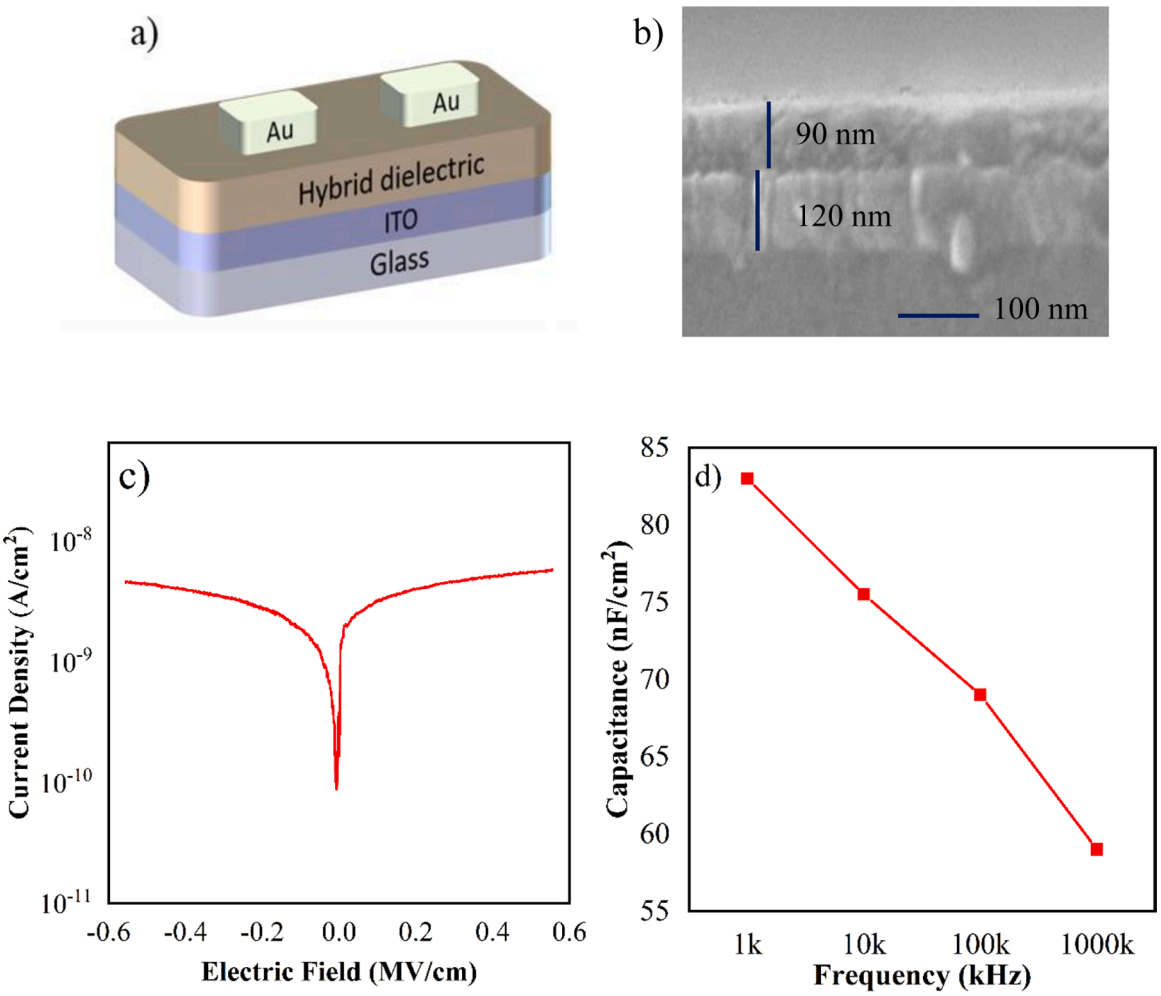

Fig. 6. a) Schematic diagram of the MIM capacitor with hybrid dielectric, b) FESEM cross-section image of the hybrid dielectric layer, c) leakage current density vs voltage and d) capacitance vs frequency measured on the MIM capacitor.

$$C = \frac{k\varepsilon_0 A}{d} \tag{3}$$

where C is the gate capacitance, d is the thickness of the hybrid dielectric, ε_0 is the permittivity of the free space and A is the area of the gold contacts. The yielded dielectric constant (k) of the hybrid dielectric film is of 8.4 at 1 kHz, 7.6 at 10 kHz, 7 at 100 kHz and 6 at 1 MHz. These values are close to others reported for low temperature solution processed hybrid dielectric [57].

In order to investigate the electrical performance of the $ZrHfO_2$-PMMA insulator in TFTs as gate dielectric, we fabricated TFTs with n-type indium oxide (In_2O_3) as active layer. Fig. 7a) shows the schematic diagram of the bottom gate and top contacts In_2O_3 TFT structure. The AFM image in Fig. 7b), measured by tapping mode at 1 kHz, shows the surface morphology of the solution processed In_2O_3 channel layer deposited on the hybrid dielectric gate layer by simple spin coating and annealed at optimized low processing temperature of 220 °C. The morphology of the semiconductor active layer is very crucial to enhance the electron charge transport in the channel layer of the device, and it was assessed by the AFM image. The RMS surface roughness of the In_2O_3 thin film obtained from this image is 1.5 nm in the scanned area of 5 × 5 μm^2. The In_2O_3 TFTs were completed with evaporated aluminum as source (S) and drain (D) electrodes with channel length (L) of 80 μm and width (W) of 500 μm. The characteristics of the electrical response of the

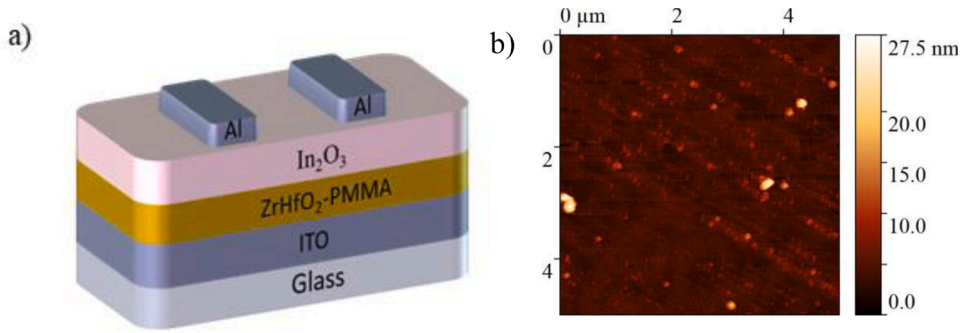

Fig. 7. a) Schematic of In_2O_3 TFT with $ZrHfO_2$-PMMA hybrid dielectric gate layer, b) AFM height image of In_2O_3 channel layer on the hybrid gate dielectric.

assembled In_2O_3 TFTs with hybrid dielectric gate layer are shown in Fig. 8. In Fig. 8a) there are depicted the output curves (I_{DS} vs V_{DS}) of the device fabricated at 220 °C, measured at several V_{GS} from 0 to 8 V, where it is observed that the drain current (I_{DS}) linearly increases in the low drain voltages (V_{DS}) region. At higher voltages, the drain current shows a clear pinch-off and excellent saturation at an applied voltage of 8 V. All the curves are not exactly converged at zero current when the drain voltage approaches to 0 V. This is due to a small non-ideal behavior mainly attributed to the high channel contact resistance at the metal electrode and the semiconductor channel layer interface of the TFT device. A similar behavior was observed in other reported works, including our previous report on a gate dielectric-based oxide TFTs [39, 40,58]. The left axis in the plots shown in Fig. 8b) displays the typical transfer curve (I_{DS} vs V_{GS}) of the In_2O_3 TFTs measured at an applied V_{DS} of 8 V in the saturation region. The I_{DS} values are plotted in log scale and the gate voltage was swept between −1 V to 10 V. The solution-processed indium oxide semiconductor layer works as n-type channel as observed in this curve. The TFT device shows low off current of 5.7×10^{-10} A, with turn-on voltage at 0 V (V_{ON}), which implies that the device is working in the enhancement mode of operation. Then, the channel drain current increases up to 1.5×10^{-4} A where the device is turned on. The TFT device performs well *ON* to *OFF* current ratio with a magnitude of 10^6. The transfer curve measurement was repeated in reverse voltage sweep direction showing the same shape with negligible hysteresis as can be observed in this graph. The obtained large $I_{on/off}$ is expected due to low-leakage current density of gate dielectric and large channel currents, which is important for high-speed displays and logic circuit applications. The Sqrt I_{DS} vs V_{GS} curve plotted in the right axis of Fig. 8b) was fitted to the Eq. (1) to extract the saturation field effect mobility (μ_{sat}) and threshold voltage (V_{th}) of the device. The dashed line in this graph shows the best linear fit. As a result, the estimated mobility is 11.2 $cm^2\ V^{-1}\ s^{-1}$, for this, the capacitance of the dielectric gate at low frequency (1 kHz) was used to avoid the overestimation. On the other hand, the resulting value for the threshold voltage was 1.7 V. We also extracted the subthreshold swing (*SS*) of the device, 0.58 V/dec, by fitting this log I_{DS} vs V_{GS} curve to the following equation:

$$SS = dV_{GS}/(dlogI_{DS}) \tag{4}$$

Furthermore, the charge trap density (D_{IT}) at the dielectric/semiconductor interface was calculated by using the below Eq. (5) [30] and the obtained D_{IT} is found to be as low as 9×10^{12} cm^{-2}.

$$D_{IT} = \left(\frac{SSlog(e)}{kT/q} - 1\right).\frac{C}{q} \tag{5}$$

In the Eq. (5), q is the electron charge, k is the Boltzmann's constant, e is the Euler's number, T is the absolute temperature and C is the capacitance per unit area (1.06×10^{-7} F/cm^2) of the hybrid dielectric layer. Such an outstanding performance of the In_2O_3TFT can be attributed to the high quality of the UV-ozone treated dielectric surface, which contains low density of traps with less non-polar groups enabling the accumulation of charge carriers at the dielectric/semiconductor interface. These results show that the electrical parameters (e.g., μ_{sat}, *S.S*, V_{th} and $I_{on/off}$) of our fully solution-processed In_2O_3 TFTs with hybrid gate dielectric are much better than our previously reported $ZrHfO_2$-PMMA hybrid dielectric layer for sputtered a-IGZO and ZnO-based metal oxide TFTs [42]. Furthermore, for comparison purposes, Table 2 summarizes the information reported about In_2O_3-based TFTs with different dielectric gate layers, mainly inorganics. Besides the electrical performance parameters, the table includes the processing temperatures of both semiconductor and dielectric layers. The information in this table corroborates that the electrical performance of our solution In_2O_3 TFTs is comparable or even better as that reported for other In_2O_3 devices with higher temperature processed inorganic gate dielectrics.

4. Conclusion

In conclusion, we developed a fully solution-processed high performance indium oxide (In_2O_3) TFT based on an improved sol-gel $ZrHfO_2$-PMMA hybrid dielectric layer. The fabrication process of the TFTs was achieved at low temperature under 220 °C. The insulating properties of the hybrid dielectric layers such as low leakage current density under 1 nA/cm^2 and the high dielectric constant of 8.4 at 1 kHz were significantly improved by filling the oxygen vacancies and reducing residual hydroxyl groups by the UV-ozone treatment. In addition, the UV-ozone treatment provides the smooth surface with low surface energy of 26.8 mJ/m^2 enabling the better interface for the deposition by solution process of the In_2O_3 semiconductor channel layer. In these conditions, the fully solution-processed bottom gate In_2O_3 TFTs featured high saturation field effect mobility (μ_{sat}) of 11.2 $cm^2.V^{-1}.s^{-1}$, high $I_{on/off}$ current ratio of 10^6, a threshold voltage of 1.7 V, and subthreshold slope of 0.58 V/dec. This work demonstrates the potential realization of fully solution processed In_2O_3 TFTs at low temperature with mechanically flexible hybrid dielectric layers, which may open new opportunities for future potential flexible oxide TFT applications.

Credit author statement

The authors contribution in the submitted work titled as $ZrHfO_2$-PMMA hybrid dielectric layers for high-performance all solution-processed In_2O_3-based TFTs following with

M.G. Syamala Rao conceptualization, methodology, manuscript writing & editing.

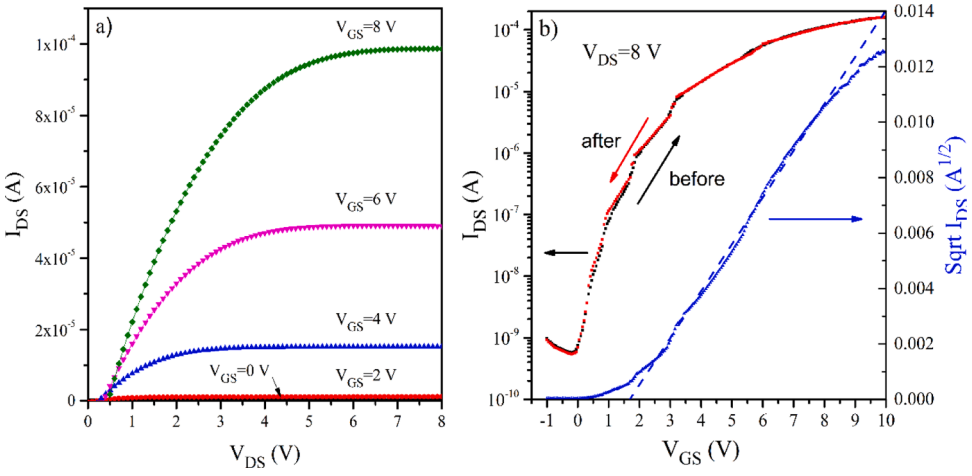

Fig. 8. Electrical response of the In_2O_3 TFT with $ZrHfO_2$-PMMA hybrid gate dielectric layer a) Output and b) Transfer characteristics.

Table 2
Electrical characteristics of solution processed In_2O_3-based TFTs with different gate insulators.

dielectric gate	sc	method	T(°C)	$\mu_{sat}(cm^2/V.\ s)$	$V_{th}(V)$	$I_{ON/OFF}$	$SS(V/dec)$	Ref.
$ZrHfO_2$-PMMA	In_2O_3	spin	200/220	11.2	1.7	10^6	0.58	This work
Al_2O_3	In_2O_3	spin	R.T/300	3.53	0.6	10^5	0.16	[2]
ZrO_2/ Al_2O_3	In_2O_3	spin	250/175	6.7	0.1	10^5	–	[36]
ZrO_2	In_2O_3	spin	300/300	4.42	0.31	10^7	0.078	[19]
GaO_x	In_2O_3	spin	500/250	3.09	0.83	10^5	0.18	[22]
$ZrAlO_x$	In_2O_3	spin	500/270	10.14	0.36	10^6	0.1	[32]
HfGdOx	In_2O_3	spin	500/270	11.2	0.58	10^6	0.10	[34]
$ZrGdO_x$	In_2O_3	spin	400/225	5.48	1.44	10^5	0.19	[35]
ZrO_x/SAM	In_2O_3	spin	150/250	7.87	0.6	10^5	0.1	[43]
HfO_2-PVP	In_2O_3	spin	200/250	2.6	0.1	10^5	0.33	[59]
SiO_2	In_2O_3	spin	-/250	4.4	4	10^8	–	[60]
Al_2O_3	In_2O_3	printing	300/150	8	–	10^6	0.4	[61]
$Y_2Al_{2-x}O_x$	In_2O_3	printing	500/250	1.3	–	10^4	0.4	[62]
Si_3N_4	In_2O_3	spin	-/275	1.28	0.84	10^6	1	[63]
SiO_2	In_2O_3	spin	-/300	6.94	5.37	10^6	0.57	[64]
Al_2O_3	In_2O_3	spin	-/300	3.5	–	10^7	–	[65]

K. Chandra Sekhar Reddy validation, resources, and manuscript writing.

J. Meza-Arroyo validation, resources, and manuscript revision.

Lakshmi N.S. Murthy results discussion, manuscript revision.

Trey B. Daunis results discussion, manuscript revision.

Maria Isabel Pintor-Monroy results discussion, manuscript revision.

Julia W.P Hsu results discussion, manuscript revision.

R. Ramirez-Bon conceptualization, results discussion, and manuscript revision.

Declaration of Competing Interest

The authors declare that they have no known competing financial interests or personal relationships that could have appeared to influence the work reported in this paper.

Acknowledgements

We would like to acknowledge Carlos Alberto Avila Herrera for his helpful technical assistance and CONACYT-Mexico for the partial financial support (Project number 271031). M.G. Syamala Rao also acknowledges the PRODEP for the support of postdoctoral fellowship. L.N. S.M. and J.W.P.H acknowledge the support of the National Science Foundation CBET-1916612. J.W.P.H also acknowledges the Texas Instruments Distinguished Chair in Nanoelectronics.

References

[1] X. Liang, L. Liu, G. Cai, P. Yang, Y. Pei, C. Liu, Evidence for pseudocapacitance and faradaic charge transfer in high-mobility thin-film transistors with solution-processed oxide dielectrics, J. Phys. Chem. Lett. 11 (2020) 2765–2771, https://doi.org/10.1021/acs.jpclett.0c00583.

[2] S.R. Bhalerao, D. Lupo, A. Zangiabadi, I. Kymissis, J. Leppaniemi, A. Alastalo, P. R. Berger, 0.6 V threshold voltage thin film transistors with solution processable indium oxide (In_2O_3) Channel and Anodized High-κ Al_2O_3 Dielectric, IEEE Electron Device Lett 40 (2019) 1112–1115, https://doi.org/10.1109/LED.2019.2918492.

[3] N. Koslowski, V. Trouillet, J.J. Schneider, Solution-processed amorphous yttrium aluminium oxide YAlx Oy and aluminum oxide AlxOy , and their functional dielectric properties and performance in thin-film transistors, J. Mater. Chem. C. (2020), https://doi.org/10.1039/d0tc01876g.

[4] J. Park, N.-.K. Cho, S.-.E. Lee, E.G. Lee, J. Lee, C. Im, H.-.J. Na, Y.S. Kim, Atmospheric-pressure plasma treatment toward high-quality solution-processed aluminum oxide gate dielectric films in thin-film transistors, Nanotechnology 30 (2019), 495702, https://doi.org/10.1088/1361-6528/ab4073.

[5] C. Zhu, A. Liu, G. Liu, G. Jiang, Y. Meng, E. Fortunato, R. Martins, F. Shan, Low-temperature, nontoxic water-induced high-: k zirconium oxide dielectrics for low-voltage, high-performance oxide thin-film transistors, J. Mater. Chem. C. 4 (2016) 10715–10721, https://doi.org/10.1039/c6tc02607a.

[6] J.W. Jo, K.H. Kim, J. Kim, S.G. Ban, Y.H. Kim, S.K. Park, High-mobility and hysteresis-free flexible oxide thin-film transistors and circuits by using bilayer sol-gel gate dielectrics, ACS Appl. Mater. Interfaces 10 (2018) 2679–2687, https://doi.org/10.1021/acsami.7b10786.

[7] J.O. Kim, J.S. Hur, D. Kim, B. Lee, J.M. Jung, H.A. Kim, U.J. Chung, S.H. Nam, Y. Hong, K.S. Park, J.K. Jeong, Network structure modification-enabled hybrid polymer dielectric film with zirconia for the stretchable transistor applications, Adv. Funct. Mater. (2020) 1–13, https://doi.org/10.1002/adfm.201906647, 1906647.

[8] W. Cai, J. Zhang, J. Wilson, J. Brownless, S. Park, L. Majewski, A. Song, Significant performance improvement of oxide thin-film transistors by a self-assembled monolayer treatment, Adv. Electron. Mater. 6 (2020), https://doi.org/10.1002/aelm.201901421.

[9] W. Cai, J. Brownless, J. Zhang, H. Li, E. Tillotson, D.G. Hopkinson, S.J. Haigh, A. Song, Solution-processed HfOx for half-volt operation of InGaZnO thin-film transistors, ACS Appl. Electron. Mater. 1 (2019) 1581–1589, https://doi.org/10.1021/acsaelm.9b00325.

[10] D. Kim, H.K. Woo, Y.M. Lee, Y. Kim, J.H. Choi, S.J. Oh, Controllable doping and passivation of ZnO thin films by surface chemistry modification to design low-cost and high-performance thin film transistors, Appl. Surf. Sci. 509 (2020) 1–7, https://doi.org/10.1016/j.apsusc.2020.145289.

[11] B.S. Yu, J.Y. Jeon, B.C. Kang, W. Lee, Y.H. Kim, T.J. Ha, Wearable 1 V operating thin-film transistors with solution-processed metal-oxide semiconductor and dielectric films fabricated by deep ultra-violet photo annealing at low temperature, Sci. Rep. 9 (2019) 1–13, https://doi.org/10.1038/s41598-019-44948-z.

[12] R.N. Bukke, N.N. Mude, J.K. Saha, J. Jang, High performance of a-IZTO TFT by purification of the semiconductor oxide precursor, Adv. Mater. Interfaces 6 (2019) 1–9, https://doi.org/10.1002/admi.201900277.

[13] N. Pal, A. Sharma, V. Acharya, N.K. Chourasia, S. Biring, B.N. Pal, Gate interface engineering for subvolt metal oxide transistor fabrication by using ion-conducting dielectric with Mn_2O_3 gate interface, ACS Appl. Electron. Mater. 2 (2020) 25–34, https://doi.org/10.1021/acsaelm.9b00641.

[14] E. Carlos, J. Leppäniemi, A. Sneck, A. Alastalo, J. Deuermeier, R. Branquinho, R. Martins, E. Fortunato, Printed, highly stable metal oxide thin-film transistors with ultra-thin high-κ oxide dielectric, Adv. Electron. Mater. 6 (2020) 1–10, https://doi.org/10.1002/aelm.201901071.

[15] W. Xu, L. Hu, C. Zhao, L. Zhang, D. Zhu, P. Cao, W. Liu, S. Han, X. Liu, F. Jia, Y. Zeng, Y. Lu, Low temperature solution-processed IGZO thin-film transistors, Appl. Surf. Sci. 455 (2018) 554–560, https://doi.org/10.1016/j.apsusc.2018.06.005.

[16] W.J. Scheideler, M.W. McPhail, R. Kumar, J. Smith, V. Subramanian, Scalable, high-performance printed InOx transistors enabled by ultraviolet-annealed printed high- k AlOx gate dielectrics, ACS Appl. Mater. Interfaces 10 (2018) 37277–37286, https://doi.org/10.1021/acsami.8b12895.

[17] T.B. Daunis, D. Barrera, G. Gutierrez-Heredia, O. Rodriguez-Lopez, J. Wang, W. E. Voit, J.W.P. Hsu, Solution-processed oxide thin film transistors on shape memory polymer enabled by photochemical self-patterning, J. Mater. Res. 33 (2018) 2454–2462, https://doi.org/10.1557/jmr.2018.296.

[18] F. Zhang, G. Liu, A. Liu, B. Shin, F. Shan, Solution-processed hafnium oxide dielectric thin films for thin-film transistors applications, Ceram. Int. 41 (2015) 13218–13223, https://doi.org/10.1016/j.ceramint.2015.07.099.

[19] L. Zhu, G. He, J. Lv, E. Fortunato, R. Martins, Fully solution-induced high performance indium oxide thin film transistors with ZrOx high-k gate dielectrics, RSC Adv 8 (2018) 16788–16799, https://doi.org/10.1039/c8ra02108b.

[20] N. Koslowski, R.C. Hoffmann, V. Trouillet, M. Bruns, S. Foro, J.J. Schneider, Synthesis, oxide formation, properties and thin film transistor properties of yttrium and aluminium oxide thin films employing a molecular-based precursor route, RSC Adv 9 (2019) 31386–31397, https://doi.org/10.1039/c9ra05348d.

[21] N. Koslowski, S. Sanctis, R.C. Hoffmann, M. Bruns, J.J. Schneider, Synthesis, dielectric properties and application in a thin film transistor device of amorphous aluminum oxide Alx Oy using a molecular based precursor route, J. Mater. Chem. C. 7 (2019) 1048–1056, https://doi.org/10.1039/c8tc04660c.

[22] L. Chen, W. Xu, W. Liu, S. Han, P. Cao, M. Fang, D. Zhu, Y. Lu, Polymer-assisted deposition of gallium oxide for thin-film transistor applications, ACS Appl. Mater. Interfaces 11 (2019) 29078–29085, https://doi.org/10.1021/acsami.9b10888.

[23] K. Everaerts, J.D. Emery, D. Jariwala, H.J. Karmel, V.K. Sangwan, P. L. Prabhumirashi, M.L. Geier, J.J. McMorrow, M.J. Bedzyk, A. Facchetti, M. C. Hersam, T.J. Marks, Ambient-processable high capacitance hafnia-organic self-assembled nanodielectrics, J. Am. Chem. Soc. 135 (2013) 8926–8939, https://doi.org/10.1021/ja4019429.

[24] J. Zhang, P. Dong, Y. Gao, C. Sheng, X. Li, Performance enhancement of ZITO thin-film transistors via graphene bridge layer by sol-gel combustion process, ACS Appl. Mater. Interfaces 7 (2015) 24103–24109, https://doi.org/10.1021/acsami.5b07148.

[25] Y.H. Kim, H. Jung, K. Lee, T.S. Yoon, H.H. Lee, Solution processed hafnium oxide doped siloxane dielectrics for a thin film transistor with reduced graphene oxide channel on flexible substrate, J. Nanosci. Nanotechnol. 17 (2017) 7423–7428, https://doi.org/10.1166/jnn.2017.14780.

[26] W. Cai, J. Brownless, J. Zhang, H. Li, E. Tillotson, D.G. Hopkinson, S.J. Haigh, A. Song, Solution-processed HfOx for half-volt operation of InGaZnO thin-film transistors, ACS Appl. Electron. Mater. 1 (2019) 1581–1589, https://doi.org/10.1021/acsaelm.9b00325.

[27] J.K. Saha, J. Jang, M.M. Billah, R.N. Bukke, Y.G. Kim, N.N. Mude, A.B. Siddik, M. M. Islam, Y. Do, M. Choi, Highly stable, nanocrystalline, ZnO thin-film transistor by spray pyrolysis using high-K dielectric, IEEE Trans. Electron Devices 67 (2020) 1021–1026, https://doi.org/10.1109/TED.2020.2969958.

[28] A. Liu, H. Zhu, Z. Guo, Y. Meng, G. Liu, E. Fortunato, R. Martins, F. Shan, Solution combustion synthesis: low-temperature processing for p-type Cu:NiO thin films for transparent electronics, Adv. Mater. (2017) 29, https://doi.org/10.1002/adma.201701599.

[29] J. Lee, M. Jae, S.Z. Hassan, D.S. Chung, Sublimation-doping with super bases for high-performance solution-processed heterojunction oxide thin film transistors, Mater. Horizons 8 (2021) 3105–3112, https://doi.org/10.1039/d1mh00929j.

[30] S.J. Park, T.J. Ha, Effects of interfacial dielectric layers on the charge transport characteristics in sol-gel based amorphous metal-oxide thin-film transistors, Thin Solid Films 708 (2020), 138113, https://doi.org/10.1016/j.tsf.2020.138113.

[31] G. He, W. Li, Z. Sun, M. Zhang, X. Chen, Potential solution-induced HfAlO dielectrics and their applications in low-voltage-operating transistors and high-gain inverters, RSC Adv. 8 (2018) 36584–36595, https://doi.org/10.1039/C8RA07813K.

[32] L. Zhu, G. He, C. Zhang, B. Yang, Y. Xia, F. Alam, Y. Zhang, Water-derived all-oxide thin-film transistors with ZrAlOx gate dielectrics and exploration in digital circuits, IEEE Trans. Electron Devices 66 (2019) 4198–4204, https://doi.org/10.1109/TED.2019.2935615.

[33] S. Bolat, P. Fuchs, S. Knobelspies, O. Temel, G.T. Sevilla, E. Gilshtein, C. Andres, I. Shorubalko, Y. Liu, G. Tröster, A.N. Tiwari, Y.E. Romanyuk, Inkjet-printed and deep-UV-annealed YAlOx dielectrics for high-performance IGZO thin-film transistors on flexible substrates, Adv. Electron. Mater. 5 (2019) 1–9, https://doi.org/10.1002/aelm.201800843.

[34] C. Zhang, G. He, Z. Fang, Y. Zhang, Y. Xia, B. Yang, W. Wang, F. Alam, J. Cui, Eco-friendly fully water-driven HfGdOx gate dielectrics and its application in thin-film transistors and logic circuits, IEEE Trans. Electron Devices 67 (2020) 1001–1008, https://doi.org/10.1109/TED.2019.2963224.

[35] L. Zhu, G. He, W. Li, B. Yang, E. Fortunato, R. Martins, Nontoxic, eco-friendly fully water-induced ternary ZrGdO dielectric for high-performance transistors and unipolar inverters, Adv. Electron. Mater. 4 (2018) 1–13, https://doi.org/10.1002/aelm.201800100.

[36] T.B. Daunis, J.M.H. Tran, J.W.P. Hsu, Effects of environmental water absorption by solution-deposited Al_2O_3 gate dielectrics on thin film transistor performance and mobility, ACS Appl. Mater. Interfaces 10 (2018) 39435–39440, https://doi.org/10.1021/acsami.8b15592.

[37] J. Li, W. Tang, Q. Wang, W. Sun, Q. Zhang, X. Guo, X. Wang, F. Yan, Solution-processable organic and hybrid gate dielectrics for printed electronics, Mater. Sci. Eng. R Rep. 127 (2018) 1–36, https://doi.org/10.1016/j.mser.2018.02.004.

[38] J.S. Hur, J.O. Kim, H.A. Kim, J.K. Jeong, Stretchable polymer gate dielectric by ultraviolet-assisted hafnium oxide doping at low temperature for high-performance indium gallium tin oxide transistors, ACS Appl. Mater. Interfaces 11 (2019) 21675–21685, https://doi.org/10.1021/acsami.9b02935.

[39] J.O. Kim, J.S. Hur, D. Kim, B. Lee, J.M. Jung, H.A. Kim, U.J. Chung, S.H. Nam, Y. Hong, K.S. Park, J.K. Jeong, Network Structure Modification-Enabled Hybrid Polymer Dielectric Film with Zirconia for the Strecheble Transistor Applications, 2019, pp. 1–13, https://doi.org/10.1002/adfm.201906647, 1906647.

[40] G.S.R. Mullapudi, G.A. Velazquez-Nevarez, C. Avila-Avendano, J.A. Torres-Ochoa, M.A. Quevedo-López, R. Ramírez-Bon, Low-temperature deposition of inorganic–organic HfO_2 –PMMA hybrid gate dielectric layers for high-mobility ZnO thin-film transistors, ACS Appl. Electron. Mater. 1 (2019) 1003–1011, https://doi.org/10.1021/acsaelm.9b00175.

[41] M.G. Syamala Rao, M.A. Pacheco-Zuñiga, L.A. Garcia-Cerda, G. Gutiérrez-Heredia, J.A. Torres Ochoa, M.A. Quevedo López, R. Ramírez-Bon, Low-temperature sol-gel $ZrHfO_2$-PMMA hybrid dielectric thin-films for metal oxide TFTs, J. Non Cryst. Solids 502 (2018) 152–158, https://doi.org/10.1016/j.jnoncrysol.2018.08.014.

[42] J. Meza-Arroyo, M.G. Syamala Rao, I. Mejia, M.A. Quevedo-López, R. Ramírez-Bon, Low temperature processing of Al_2O_3-GPTMS-PMMA hybrid films with applications to high-performance ZnO thin-film transistors, Appl. Surf. Sci. 467 (2019) 456–461, https://doi.org/10.1016/j.apsusc.2018.10.170, 468.

[43] M.G.S. Rao, A. Sánchez-Martinez, G. Gutiérrez-Heredia, M.A. Quevedo-López, R. Ramírez-Bon, Sol-gel derived low temperature HfO_2-GPTMS hybrid gate dielectric for a-IGZO thin-film transistors (TFTs), Ceram. Int. 44 (2018) 16428–16434, https://doi.org/10.1016/j.ceramint.2018.06.056.

[44] S. Sun, L. Lan, Y. Li, H. Ning, R. Yao, L. Wang, J. Peng, Stable ambipolar organic–inorganic heterojunction field effect transistors and invertors with CYTOP inter layer, RSC. Adv. 7 (2017) 5966, doi. 10.1039/c6ra26817j.

[45] H.R. Byun, E.A. You, Y.G. Ha, Multifunctional hybrid multilayer gate dielectrics with tunable surface energy for ultralow-power organic and amorphous oxide thin-film transistors, ACS Appl. Mater. Interfaces 9 (2017) 7347–7354, doi.10.1021.acsami.6b 15798.

[46] Y.H. Kim, M. Kim, S. Oh, H. Jung, Y. Kim, T.S. Yoon, Y.S. Kim, H. HoLee, Organic memory device with polyaniline nanoparticles embedded as charging elements, Appl. Phys. Lett. (2012) 100, https://doi.org/10.1063/1.4704571.

[47] J.M. Jung, D.H. Kim, J.S. Hur, H.A. Kim, J.O. Kim, J.K. Jeong, Acrylate-based nanocomposite zirconium-dispersed polymer dielectric for flexible oxide thin-film transistors with a curvature radius of 2 mm, Org. Electron. 98 (2021), 106302, https://doi.org/10.1016/j.orgel.2021.106302.

[48] L.Y. Cui, R.C. Zeng, X.X. Zhu, T.T. Pang, S.Q. Li, F. Zhang, Corrosion resistance of biodegradable polymeric layer-by-layer coatings on magnesium alloy AZ31, Front. Mater. Sci. 10 (2016) 134–146, https://doi.org/10.1007/s11706-016-0332-1.

[49] Q. Lu, R. Huang, X. Lan, X. Chi, C. Lu, C. Li, Z. Wu, J. Li, G. Han, P. Yan, Amazing diffusion depth of ultra-thin hafnium oxide film grown on n-type silicon by lower temperature atomic layer deposition, Mater. Lett. 169 (2016) 164–167, https://doi.org/10.1016/j.matlet.2016.01.087.

[50] T.L. Duan, L. Pan, Z. Zhang, E.S. Tok, J.S. Pan, Characterization of the electronic structure and thermal stability of $HfO_2/SiO_2/Si$ gate dielectric stack, Surf. Interface Anal. 49 (2017) 776–780, https://doi.org/10.1002/sia.6222.

[51] S.V. Harb, A. Trentin, M.C. Uvida, M. Magnani, S.H. Pulcinelli, C.V. Santilli, P. Hammer, A comparative study on PMMA-TiO_2 and PMMA-ZrO_2 protective coatings, Prog. Org. Coatings (2020) 140, https://doi.org/10.1016/j.porgcoat.2019.105477.

[52] M.S. de Urquijo-Ventura, M.G.S. Rao, S. Meraz-Davila, J.A.T. Ochoa, M. A. Quevedo-Lopez, R. Ramirez-Bon, PVP-SiO_2 and PVP-TiO_2 hybrid films for dielectric gate applications in CdS-based thin film transistors, Polymer (Guildf) 191 (2020), 122261, https://doi.org/10.1016/j.polymer.2020.122261.

[53] X. Sun, C.A. Di, Y. Liu, Engineering of the dielectric-semiconductor interface in organic field-effect transistors, J. Mater. Chem. 20 (2010) 2599–2611, https://doi.org/10.1039/b921449f.

[54] A. Kyndiah, A. Ablat, S. Guyot-Reeb, T. Schultz, F. Zu, N. Koch, P. Amsalem, S. Chiodini, T. Yilmaz Alic, Y. Topal, M. Kus, L. Hirsch, S. Fasquel, M. Abbas, A multifunctional interlayer for solution processed high performance indium oxide transistors, Sci. Rep. 8 (2018) 1–7, https://doi.org/10.1038/s41598-018-29220-0.

[55] Y.M. Park, J. Daniel, M. Heeney, A. Salleo, Room-temperature fabrication of ultrathin oxide gate dielectric for low-voltage operation of organic field-effect transistors, Adv. Mater. 23 (2011) 971–974, https://doi.org/10.1002/adma.201003641.

[56] C.L. Fan, Y.Z. Lin, C.H. Huang, Combined scheme of UV-Ozone and HDMS treatment on gate insulator for performance improvement of a low-temperature-processed bottom-contact OTFT, Semicond. Sci. Technol. 26 (2011), 045006, https://doi.org/10.1088/0268-1242/26/4/045006.

[57] D. Sánchez-Ahumada, L.J. Verastica-Ward, M. Orozco, D. Vargas-Hernández, A. Castro-Beltrán, R. Ramirez-Bon, C.G. Alvarado-Beltrán, In-situ low-temperature synthesis of PS-ZrO2 hybrid films and their characterization for high-k gate dielectric application, Prog. Org. Coatings (2021) 154, https://doi.org/10.1016/j.porgcoat.2021.106188.

[58] S. Park, K.H. Kim, J.W. Jo, S. Sung, K.T. Kim, W.J. Lee, J. Kim, J.J. Kim, G.R. Yi, Y. H. Kim, M.H. Yoon, S.K. Park, In-depth studies of rapid photochemical activation of Various sol-gel metal oxide films for flexible transparent electronics, Adv. Fun. Mater. (2015) 1–9, https://doi.org/10.1002/adfm.201500545.

[59] M.G. Syamala Rao, J. Meza-Arroyo, K. Chandra Sekhar Reddy, Lakshmi N. S. Murthy, M.S. de Urquijo-Ventura, F. Garibay-Martínez, Julia.W.P. Hsu, R. Ramirez-Bon, Tuning the electrical performance of solution-processed In_2O_3 TFTs by low-temperature with HfO_2-PVP hybrid dielectric, Mater. Today Commun. 26 (2021), 102120, https://doi.org/10.1016/j.mtcomm.2021.102120.

[60] T.B. Daunis, W Xu, S Thampy, M Valdez, Julia.W.P. Hsu, Effect of atmosphere composition during ultra-violet light patterning of solution deposited In_2O_3 thin film transistors, Thin Solid Films 731 (2021), 138829, https://doi.org/10.1016/j.tsf.2021.138829.

[61] J. Leppäniemi, O.H. Huttunen, H. Majumdar, A. Alastalo, Flexography-printed In2O3 semiconductor layers for high-mobility thin-film transistors on flexible plastic substrate, Adv. Mater. 27 (2015) 7168–7175, https://doi.org/10.1002/adma.201502569.

[62] L. Gillan, S. Li, J. Lahtinen, C.H. Chang, A. Alastalo, J. Leppäniemi, Inkjet-printed ternary oxide dielectric and doped interface layer for metal-oxide thin-film transistors with low voltage operation, Adv. Mater. Interfaces 8 (2021) 1–10, https://doi.org/10.1002/admi.202100728.

[63] R. Yao, X. Fu, W. Li, S. Zhou, H. Ning, B. Tang, J. Wei, X. Cao, W. Xu, J. Peng, Bias stress stability of solution-processed nano indium oxide thin film transistor, Micromachines (Basel) 12 (2021) 1–9, https://doi.org/10.3390/mi12020111.

[64] D. Li, J. Du, Y. Tang, K. Liang, Y. Wang, H. Ren, R. Wang, L. Meng, B. Zhu, Y. Li, Flexible and air-stable near-infrared sensors based on solution-processed inorganic–organic hybrid phototransistors, Adv. Funct. Mater. 31 (2021) 1–10, https://doi.org/10.1002/adfm.202105887.

[65] J. Leppäniemi, A. Sneck, Y. Kusaka, N. Fukuda, A. Alastalo, Reverse-offset printing of metal-nitrate-based metal oxide semiconductor ink for flexible TFTs, Adv. Electron. Mater. 5 (2019) 1–7, https://doi.org/10.1002/aelm.201900272.